

# Creating a Contact Binary via Spacecraft Impact to Near-Earth Binary Asteroid (350751) 2002 AW

Colby C. Merrill<sup>a</sup>, Carl J. Geiger<sup>a</sup>, Abu T. M. Tahsin<sup>a</sup>, Dmitry Savransky<sup>a</sup>, Mason Peck<sup>a</sup>

<sup>a</sup>*Sibley School of Mechanical and Aerospace Engineering Cornell University 124 Hoy Rd Ithaca NY 14853 USA*

---

## Abstract

Contact binary asteroids are ubiquitous in the solar system: the Kuiper belt, main belt, and near-Earth populations all house these complex aggregates. Although contact binaries account for approximately 10% of small bodies in the Solar System, the formation of one has yet to be observed. We present a preliminary mission design to create a contact binary asteroid and observe its formation using a binary NEO system, a kinetic impactor, and an observer spacecraft. Not only does this mission address an important gap in planetary science, it also serves the planetary defense community: it will further demonstrate planetary defense technology to provide unique observation opportunities. A binary system offers a convenient natural laboratory for this mission, as the ability to form a contact binary using a kinetic impactor depends greatly on the size of the target and the proximity to its parent body. From among all known binary near-Earth objects, binary asteroid system (350751) 2002 AW was chosen for this case study. A spacecraft can achieve rendezvous with this system from low-Earth orbit with a total  $\Delta V = 4.3$  km/s. The system also includes a 50 meter secondary (the lower bound of asteroid size for which a kinetic impactor might be used). A pair of spacecraft launch on the same launch vehicle and separate before asteroid impact. The two spacecraft are (1) an impactor that has been adapted from the DART spacecraft and (2) an observer spacecraft that will rendezvous with the binary system and observe the creation of the contact binary. The spacecraft impact must be designed such that it redirects the secondary into a collision course with the primary while not catastrophically disrupting the target asteroid. Impact parameters such as angle of impact, catastrophic disruption limit, and the  $\beta$  factor have been considered. Among other design decisions, we present our target-selection methodology, launch-vehicle considerations, and launch window opportunities.

*Keywords:* planetary defense, binary asteroid, contact binary, near-Earth object, asteroid deflection, kinetic impactor

---

## 1. Introduction

### 1.1. Binary Asteroid Systems & Contact Binaries

Approximately 16% of near-Earth objects exist in binary, triple, or even quadruple systems where, generally, a more massive asteroid is orbited by less massive asteroids called “moonlets” or “secondaries” [1, 2]. The irregular shape and relatively low mass of asteroids allows for small perturbations to greatly alter the orbits of the secondaries in these systems, leading to complex orbits. Among other perturbation effects, the Binary Yarkovsky-O’Keefe-Radzievskii-Paddack (BYORP) effect is particularly prominent, as it can cause the lifetime of a binary system to be lower than  $10^5$  years [3, 4].

One product of the BYORP effect is the creation of contact binaries, which are objects formed from one or more distinct objects impacting each other at low relative speeds. Contact binaries are ubiquitous in every part of the solar system: Kuiper belt object 486958 Arrokoth imaged by NASA’s New Horizons, comet 67P/Churyumov-Gerasimenko explored by ESA’s Rosetta, and near-Earth object (NEO) 25143 Itokawa sampled by JAXA’s Hayabusa are all likely contact binaries [5, 6, 7, 8]. These bodies, shown in Figure 1, represent some contact binary shapes and illustrate how unique each one is. These three bodies may all be contact binaries, but their formation processes are unlikely to be the same. Approximately 10% of all small solar

system bodies are expected to be contact binaries [9, 10, 11]. Despite their relative prominence in the Solar System, the formation of a contact binary has never been observed. The mission designs in this paper would provide the unique opportunity to observe contact binary formation and do so while using heritage technology.

The BYORP effect is understood to be the primary driver toward contact binary creation, but contact binary formation is not constrained to this one process [12, 13, 14]. Contact binaries can also be created if there is a relative contact speed between two bodies on the order of their mutual escape velocity [15]. Any greater than this relative contact speed, and the two bodies will impact and fail to form an amalgam, but instead glance off each other or, in cases of highly energetic collisions, catastrophically disrupt [16]. The resulting shapes of these bodies is highly dependent on the impact velocity and angle of impact, with more head-on collisions resulting in more cohesive amalgams and lower angles of impact creating bi-lobed bodies where both previously distinct bodies nearly retain their original shape [15].

Combining the statistics for contact binaries and binary systems, it is expected that they account for about 25% of small bodies in the near-Earth population. This means that 25% of the hazardous asteroids to Earth may be irregularly shaped (i.e.

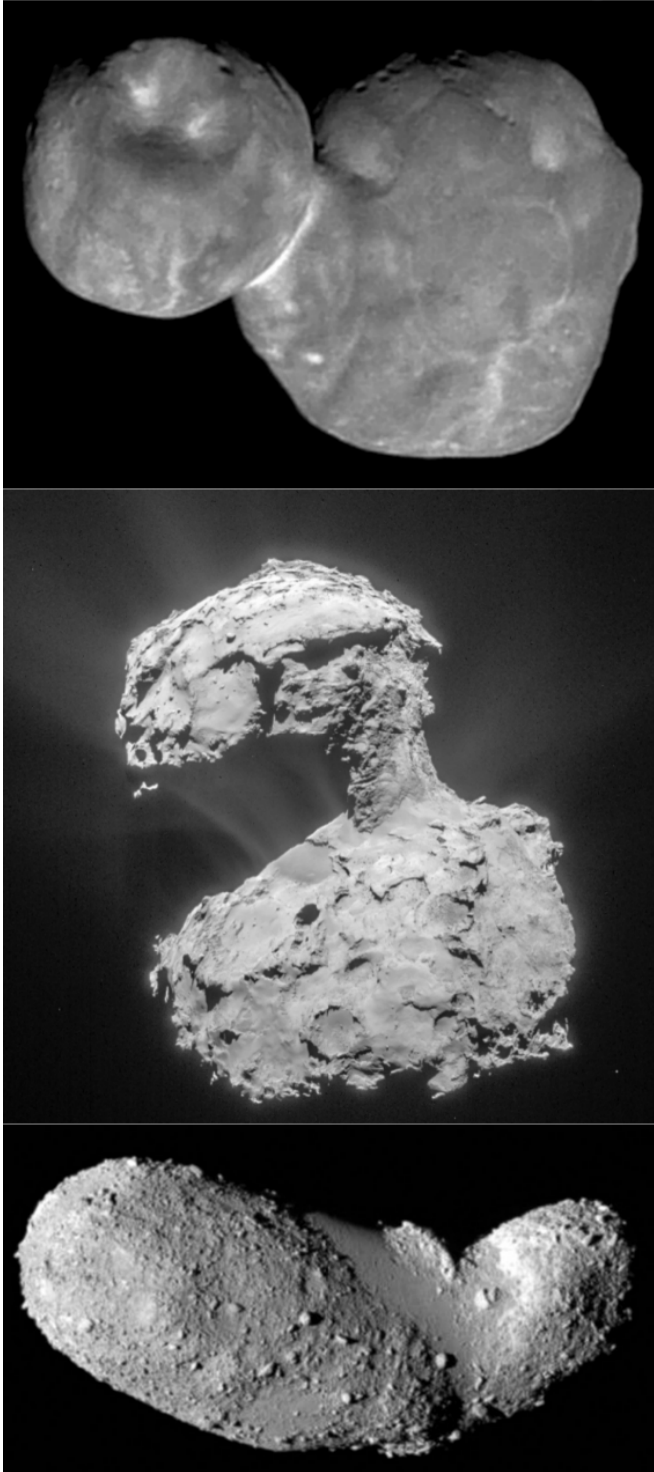


Figure 1: Arrokoth (top), 67P/Churyumov-Gerasimenko (center), and Itokawa (bottom). Images courtesy of NASA, ESA, and JAXA.

questions arise as to where a kinetic impactor should aim to effectively deflect the body) or have a secondary (i.e. questions arise as to how to efficiently deflect both bodies). Beyond providing detailed observations of contact binary formation, this mission provides a mitigation strategy for small binary systems if they pose a threat to Earth where a kinetic impact to the secondary could simultaneously combine the primary and

secondary into a single body and remove mass from the system.

### 1.2. Kinetic Impact to Small Bodies

Impacting an asteroid with a kinetic impactor reproduces the effects of high energy collisions of small Solar System bodies. Interestingly, it is most likely that the spacecraft’s imparted momentum to the target body will be multiplied. That is, if a perfectly inelastic collision predicts 1 mm/s of change in a target’s velocity, the target would likely experience  $> 1$  mm/s of velocity change. This surprising result is caused by the ejecta streams that result from high energy impacts. During a collision, mass will be excavated and removed from a target and much of it will exit the target at non-negligible speeds. For this mission and planetary defense missions that use kinetic impactor technology, this behavior means that to precisely describe the momentum imparted to a target, one must know the individual momentum of each ejected particle and sum up that momentum. Rather than attempt do this, we instead use the multiplicative momentum factor,  $\beta$  [17, 18, 19]. The  $\beta$  factor multiplies the momentum imparted to a target from an impactor by accounting for the momentum of the ejecta excavated by the impact event.  $\beta < 1$  means less momentum was imparted to the target than an inelastic collision and  $\beta = 1$  means that a collision is fully inelastic. A  $\beta \leq 1$  is unlikely for high energy impacts, and instead  $\beta > 1$  is an expectation when using a kinetic impactor [20].  $\beta > 2$  indicates that most of the momentum imparted to the target was supplied by ejecta rather than the kinetic impactor, as was true of the DART mission and will likely be true of this mission [21].

### 1.3. Mission Architecture

The NASA DART spacecraft successfully impacted Dimorphos on September 26, 2022 [21, 22, 23, 24]. This mission was Earth’s first asteroid deflection mission, and the results and technology of the DART mission will be utilized throughout this paper to further develop this mission. The DART mission used a kinetic impactor to alter the orbit of the secondary body in a binary asteroid system, with the expressed goal of deflecting the asteroid and measuring the momentum imparted to it [21]. Our goal is not only to deflect the asteroid with a kinetic impactor but to cause the secondary to meet the primary asteroid body and form a contact binary. The mission architecture outlined here uses a mission plan that was proposed previously for measuring asteroid deflections [25]. Here, we adapt this architecture to the binary-system target for the following operations concept:

1. The observer and impactor launch together on a single launch vehicle and arrive on heliocentric orbit via direct injection.
2. The two spacecraft separate when coasting in the heliocentric orbit. Along the coasting phase, the impactor maneuvers to delay its approach to the system.
3. The observer performs a rendezvous burn with the binary system.

4. The observer characterizes the two bodies, providing insight into their orbits, masses, densities, shapes, and surfaces.
5. The impactor adjusts its orbit using the data provided by the observer to optimize contact binary creation. It impacts the secondary.
6. The observer images the contact binary formation and provides data on the ejecta profile, interior of the secondary, and effectiveness of impact. After the impact, the observer's primary goal is to characterize the impact and gather more data about the system, especially the interior of the secondary.

#### 1.4. Assumptions and Constraints

We model the primary and secondary as spheres, a conservative assumption because most likely the asteroids would impact along their long axes. The long axes of the asteroids are, generally, in the plane of their motion in binary systems; so, treating the asteroids as spheres also reduces complexity. We assume that the asteroid that the spacecraft impacting is a rubble pile, as is expected of most asteroids in the size range we investigate [26]. We assume that all secondaries in this study are in circular orbits around their primary unless better data is available. The final, significant assumption that we make is that the plane that the secondary asteroid rotates around the primary on is the same plane with which the impactor spacecraft approaches such that all momentum imparted to the secondary will be in the plane of its current motion. That is, there is no inclination between the impactor spacecraft and rotation of the secondary, and so we do not account for a pre-impact inclination change maneuver. We do, however, provide propellant contingency to account for the possibility of this burn. This assumption acknowledges that the inclination of the secondary's orbit unknown for this system, and yet such a maneuver is likely insignificant even if it were required.

We constrain the search for binary systems to the near-Earth population because rendezvous with these objects require less propellant, which means the observer spacecraft can arrive with more mass and therefore perform more science. The sizes of spacecraft that we use are also constrained. The observer spacecraft's mass shall be no greater than 420 kg, the mass of the ESA AIM spacecraft with a 33% mass contingency [27]. The impactor spacecraft's impacting mass is 483 kg, which is identical to the estimated dry mass of the DART spacecraft [28]. Our expected dry mass will be lower than this, as we discard much of the solar arrays and electric propulsion mass and outfit the spacecraft with a leaner chemical thruster unit. However, we still use this value for the impacting mass because there will also be some mass remaining from necessary attitude control thrusting and final approach burns for path correction.

## 2. Mission Design

### 2.1. Binary System Selection

In order to obtain launch windows and generate a first-cut approximation of total  $\Delta V$  for this mission, we used the JPL

small body mission design tool [30]. However, the overall minimum  $\Delta V$  transfer did not fully determine which binary asteroid system we selected. We also consider what impact speed is necessary to lower the orbit of the secondary to impact the primary. For example, the Didymos-Dimorphos system could not be chosen because it requires unattainable relative velocities in order to achieve this desired mission result, despite having reasonable total  $\Delta V$  transfers. Therefore, all binary systems near to or greater than the Didymos system's size were excluded from consideration. We include the Didymos system in Tables 1 and 2 as a reference for what was excluded from the search. We used the assumption of a fully inelastic collision to determine if a system was worth considering, as this gives a good approximation of the order of magnitude for the necessary impact speed.

The known parameters for each system are the diameter of the primary,  $D_p$ , diameter of the secondary,  $D_s$ , pre-impact semi-major axis,  $a_i$ , and period of secondary's orbit,  $T$ . Density,  $\rho$ , is

$$\rho = \frac{6\mu}{\pi G (D_p^3 + D_s^3)} \quad (1)$$

and is assumed to be equal for the primary and secondary bodies.  $G$  is the gravitational constant and  $\mu$  is the system's standard gravitational parameter. We then define the radius of impact,  $r_{imp}$  as

$$r_{imp} = \frac{D_s + D_p}{2} \quad (2)$$

and this is used as the radius of periapsis for the minimum and maximum momentum transfer cases. Because we now have an apoapsis,  $a_i$ , and periapsis,  $r_{imp}$ , we can define

$$a_{f,max} = \frac{a_i + r_{imp}}{2} \quad (3)$$

which is the maximum post-impact semi-major axis for an impact event. We now determine the post-impact speed of the secondary

$$V_f = \sqrt{\frac{2\mu}{a_i} - \frac{\mu}{a_{f,max}}} \quad (4)$$

which is either perfectly parallel or antiparallel to the secondary's initial velocity. In order to account for these two cases, we must. We now define  $\delta V$  as

$$\delta V = \left| \pm \sqrt{\frac{2\mu}{a_i} - \frac{\mu}{a_{f,max}}} - \sqrt{\frac{\mu}{a_i}} \right| = |\pm V_f - V_i| \quad (5)$$

which is the change in speed of the secondary caused by the impact.  $V_i$  is the speed of the secondary before impact.  $\delta V$  has two solutions because in the bounding cases of maximum and minimum velocity change, the secondary will either continue along its current path (+ case) or move opposite its initial path and with the same final speed (- case). The mass of the secondary is found via

$$m_s = \frac{\pi D_s^3 \rho}{6} \quad (6)$$

Table 1: Physical parameters of binary system candidates for impact-induced contact binary creation. All data is derived or provided by Johnston’s archive [29]. The Didymos system is not a target candidate but is listed to emphasize which systems cannot be considered for this mission design.

Name	Primary Diameter (m)	Secondary Diameter (m)	Semi-Major Axis (m)	Period (days)
Didymos	780	170	1190	0.4971
1990 OS	300	50	600	0.875
1999 RM45	165	74	290	0.6852
2000 UG11	260	130	426	0.7667
2002 AW	230	50	520	1.047
2002 TY57	330	60	420	0.4485
2003 SS84	120	60	270	1
2003 UX34	280	100	460	0.625
2004 BL86	320	70	500	0.6
2006 GY2	400	80	500	0.487
2009 FD	150	90	250	0.6
2014 WZ120	300	100	500	0.56938
2017 RV1	300	100	470	0.5896
2018 TF3	270	60	350	0.438

assuming a perfect sphere. The minimum and maximum values for the spacecraft’s relative speed to the secondary asteroid are given by

$$V_{sc} = \delta V \frac{m_s}{m_{sc}} \quad (7)$$

where  $m_{sc}$  is the mass of the impactor. We also give this equation in terms of only known parameters and constants as

$$V_{sc} = \frac{8\pi^3 D_s^3 a_i^4}{T^3 m_{sc} G (D_p^3 + D_s^3)} \left| \pm \sqrt{\frac{2D_p + 2D_s}{2a_i + D_p + D_s} - 1} \right| \quad (8)$$

to help show how system parameters affect the  $V_{sc}$  values. Values for maximum and minimum  $V_{sc}$  for each candidate system are shown in Table 2. The variable  $V_\infty$  is used to represent a spacecraft’s speed if it were to be moved infinitely far from a gravity source with its current energy such that there was no potential energy. In these systems, the gravitational energy provided by the asteroid system is effectively negligible with respect to the spacecraft’s kinetic energy which results in  $V_\infty$  being nearly identical to  $V_{sc}$ . For example, in the system 2002 AW,  $V_{sc}$  was 2.3E-8% larger than  $V_\infty$ . Because of this minute difference, we approximate the relative speed of impact as  $V_\infty$ .

The data in Table 2 motivate selecting the system (350751) 2002 AW (hereafter referred to as 2002 AW) [29, 31]. This system meets two distinct criteria: the  $V_\infty$  value required to create the the contact binary is readily attainable and a rendezvous orbit with the system requires a low total  $\Delta V$ . If only accounting for the most attainable  $V_\infty$  value, we would select system 2003 SS84. However, to rendezvous with this system would require a total mission  $\Delta V$  more than double that of 2002 AW. The total  $\Delta V$  value is more important to us because a lower  $\Delta V$  means a more massive and capable observer spacecraft, on which the data-gathering is dependent. If we were to use any launch vehicle and be free from mass constraints, other systems would be of greater interest and other criteria would be more important. We would still need an attainable  $V_\infty$  value but we could then look at maximizing the range of  $\beta$  values. That is, maximizing the chance that the binary system is created after impact.  $\beta$  represents the greatest level of uncertainty in this mission but we

discuss our results in Section 4.2 and how that relates to mission success. From Table 2, 2018 TF3 and 2009 FD would be excellent options for maximizing the range of  $\beta$  values. Both of these systems have their maximum  $V_\infty$  more than 9 times greater than their respective  $V_\infty$ . This means that if the impactor spacecraft were to impact exactly at the minimum  $V_\infty$ , any  $\beta$  between 1 and 9 would result in collision. Our selected target has a maximum  $V_\infty$  4.73 times greater than its minimum  $V_\infty$ , which means that there is smaller range of  $\beta$  values for which an impact will form a contact binary. We use 2002 AW for this case study because of its convenient total  $\Delta V$  but we recognize that, while we determine it to be the optimal target for this mission iteration, it is likely not the optimal target among all possible binary systems.

## 2.2. Launch Window and $\Delta V$ Requirement

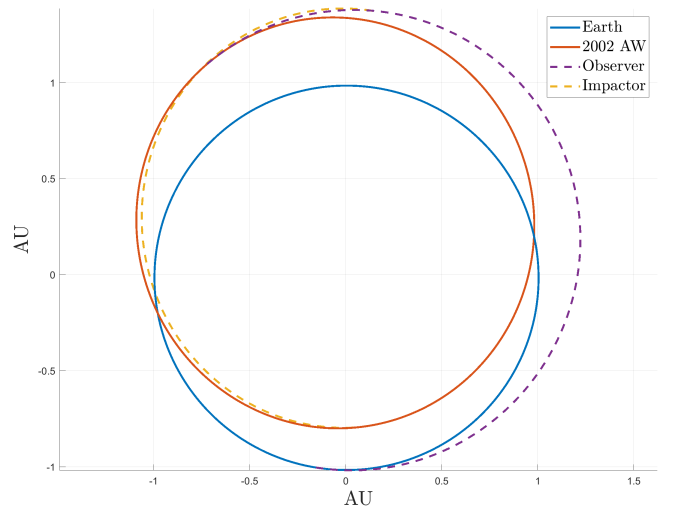


Figure 2: The specified transfer orbit to achieve the mission. The x and y axis are measured in astronomical units. 1 astronomical unit (AU) = 149597870.691 km.

The trajectory has a departure date of June 12, 2034 on a Falcon 9 launch vehicle with a  $C3 = 5.852 \text{ km}^2/\text{s}^2$ . The impactor spacecraft departs from the heliocentric rendezvous orbit

Table 2: Assuming a fully inelastic collision and a 483 kg impactor spacecraft, the relative velocities required to carry out this mission are listed. Also included is the minimum  $\Delta V$  transfer required for a rendezvous mission to the system before 2040. Data acquired using the JPL small body mission design tool [30]. The Didymos system is not a target candidate but is listed to emphasize which systems cannot be considered for this mission design.

Name	Min. $V_\infty$ Required (km/s)	Max. $V_\infty$ Allowed (km/s)	Min. Total $\Delta V$ (km/s)
Didymos	488.2	3503	6.2
1990 OS	3.49	17.78	6.5
1999 RM45	5.12	38.28	13.5
2000 UG11	20.10	173.6	10.0
2002 AW	2.69	12.76	4.3
2002 TY57	5.01	44.16	10.3
2003 SS84	2.06	12.03	8.9
2003 UX34	22.44	168.2	11.5
2004 BL86	8.97	62.54	12.6
2006 GY2	9.97	92.50	11.1
2009 FD	7.46	69.19	8.6
2014 WZ120	35.21	253.3	14.5
2017 RV1	23.06	179.8	8.5
2018 TF3	4.61	41.64	11.9

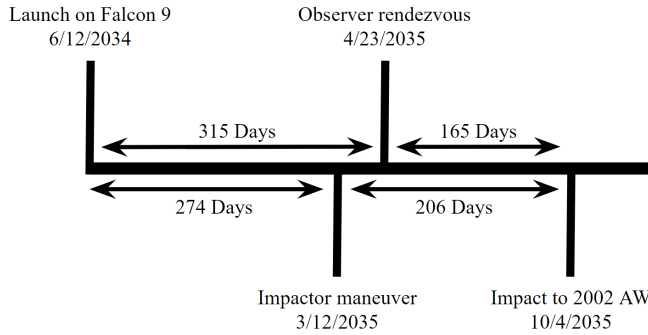


Figure 3: Timeline of key mission events. The line beyond the impact indicates extended mission duration, as the observer will continue to image the system beyond impact.

on March 12, 2035 where it performs a 2.359 km/s burn so that the observer spacecraft can fully characterize the system before the impact occurs. This allows the observer spacecraft to rendezvous with 2002 AW well before impact, as the observer will arrive with  $V_\infty = 1.894$  km/s and 165 days before impact. The total mission  $\Delta V = 4.313$  km/s for the observer. The impactor arrives with  $V_\infty = 2.391$  km/s, which we take as the impacting velocity.

### 2.3. Launch Vehicle Selection

Table 3 represents the launch vehicles that could perform this mission if it needed to be launched this year. It does not represent the launch vehicles that will necessarily be available in 2034 but does provide a basis for what could support the mission. The mission will use a Falcon 9 rocket as its launch vehicle. With a  $C3 = 5.852$  km<sup>2</sup>/s<sup>2</sup>, the Falcon 9 has a 2655 kg payload capability (for ASDS landing) according to a NASA Launch Services Program Launch Vehicle Performance Website performance query. Not only was it the launch vehicle that the DART mission relied on, but it is also a less expensive launch vehicle because of its reusability. As explained in Section 2.4, the payload mass for this mission (including significant contingency) is 2496 kg, so the Falcon 9's 2655 kg limit

is sufficient for this mission design.

Table 3: The payload masses of different launch vehicles for  $C3 = 5.8516$  km<sup>2</sup>/s<sup>2</sup>.

Vehicle	Version	Payload Mass [kg]
Falcon 9	Full Thrust, RTLS	1255
Antares	232	1455
Falcon 9	Full Thrust, ASDS	2655
Vulcan	VC2	5230
Falcon Heavy	Recovery	5735
New Glenn	New Glenn	6115
Vulcan	VC4	7700
Vulcan	VC6	9815
Falcon Heavy	Expendable	13395

### 2.4. Technology to be Utilized

The technology risk for this mission is low. It can incorporate technologies that have already flown or are being developed as parts of future missions—i.e. TRL 5 or higher. Specifically, we use the DART spacecraft as a model for the impactor in this mission, but with some key differences. This mission uses a modified version of the DART spacecraft. The spacecraft was 630 kg at launch and impacted Dimorphos at 579 kg after expending propellant and ejecting LICIAcube, its CubeSat companion. The impact mass of the impactor we use in this paper is 483 kg, identical to the dry mass of the DART spacecraft, which is the spacecraft's dry mass plus 50 kg of unused chemical propellant. The baseline mission does not use electric propulsion but, instead, uses chemical thrusters. This choice reduces the mass of solar arrays, which reduces inertia and therefore benefits the attitude-control (ACS) subsystem: the reduction leads to lighter ACS hardware and permits higher-bandwidth attitude control. Roll-out solar arrays, like the DART spacecraft used, sacrifice some maneuverability for launch volume. While this choice made sense for DART, which requires more power, it is not necessary here. A camera similar to DRACO, baselined

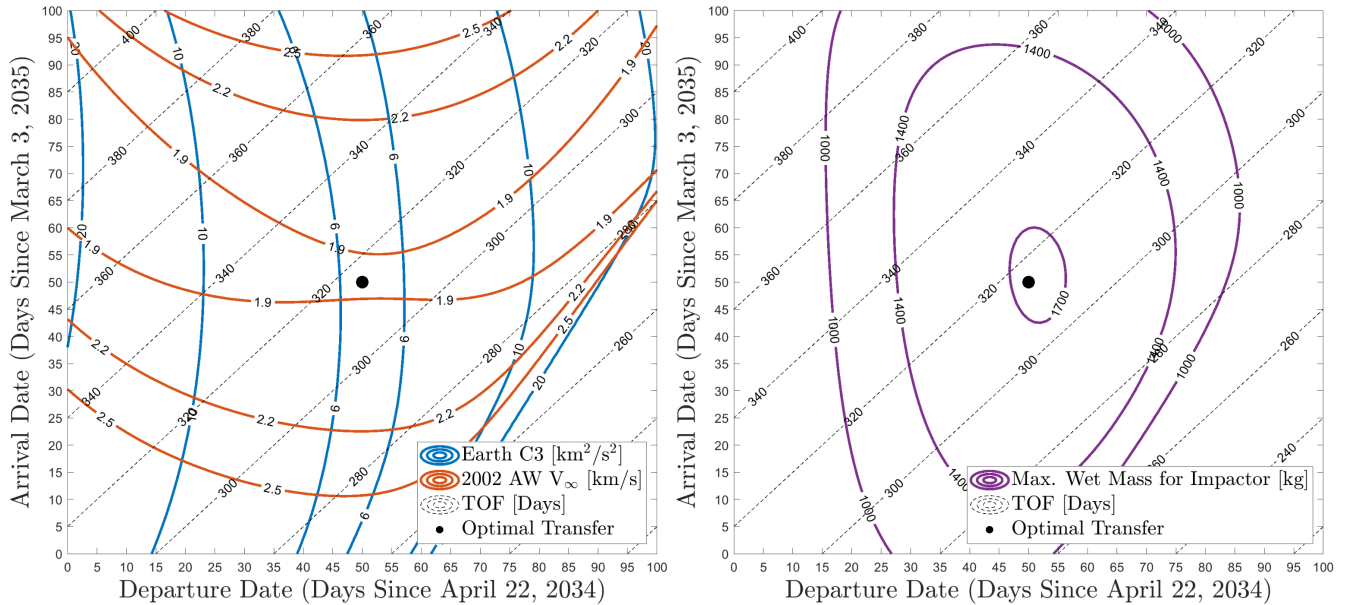


Figure 4: Earth to asteroid 2002 AW porkchop plots. The left plot details the Earth C3 and  $V_\infty$  at 2002 AW for the observer spacecraft. The right plot shows the total wet mass that the impactor spacecraft can have for these transfers from LEO to rendezvous with 2002 AW. It is created assuming a Falcon 9 will be used as the launch vehicle. The optimal transfer maximizes the maximum wet mass for the impactor.

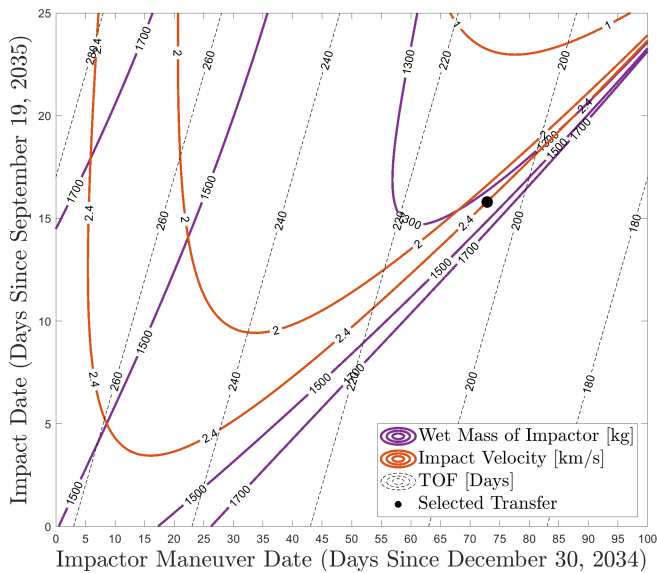


Figure 5: Impactor porkchop plot. The selected transfer is at a point where: (1) the impact to the secondary has a high chance to produce the contact binary and (2) the wet mass of the impactor is less than the maximum provided by the optimal transfer in Figure 4. There are many points in this figure where one of the two criteria are met, but both are necessary. The selected transfer point has a  $V_\infty = 2.4$  km/s (an impact velocity with a high likelihood of contact binary production for our impactor spacecraft) and minimizes the required impactor spacecraft mass for that impact velocity.

on DART, could provide optical navigation here. Though Dimorphos and Didymos are much larger than 2002 AW, DART approached them much faster than would be the case for this mission (6.14 km/s versus 2.39 km/s) [32]. Therefore, the target is visible for less time than DART could image Dimorphos, but this difference should not present a significant issue for navigation.

The observer spacecraft is inspired by the ESA AIM spacecraft, which was intended to characterize the Didymos system before DART impacted and then measure the effects of the im-

pector. The AIM mission did not occur, but the spacecraft was partially redesigned and became the Hera mission, which will instead obtain detailed data about the post-impact Didymos system [33]. The AIM spacecraft's dry mass is estimated to be 420 kg (including a 33% mass contingency) which is the mass we use for our observer [27]. AIM's payload is designed specifically to characterize a binary asteroid system before impact: low- and high-frequency radar instruments to measure the interior of the body, imaging ability to scan the entire surface, and thermal measurement of the surface are all capabilities of the AIM spacecraft [34].

Shape models of the secondary will be used to pinpoint the optimal impact area before the impact occurs. This realtime data will benefit from information collected on the target asteroid by the Goldstone Radar, which will be able to observe it for multiple years before the proposed launch date. That information includes preliminary determinations of the shapes of the primary and secondary [35]. The AIM spacecraft was meant to arrive at the Didymos system 130 days before impact and to characterize the secondary fully in that time. Not only are the instruments on AIM suitable for the proposed observer, the objectives for AIM are also nearly identical. The proposed observer also has more time, 165 days compared to 130, to characterize objects with much less surface area than those in the Didymos system. So, this observer should be highly capable. It will have the additional objective of imaging the aftermath of the collision and formation of the contact binary, but the timeline for these observations will be identical to those for the DART system, as the timescale of ejecta evolution (something that AIM was meant to observe) is much greater than the timescale for our contact binary creation [22].

## 2.5. Data to be Collected

The observer spacecraft will map the interior and exterior of the secondary using high- and low-frequency radar before im-

Table 4: The mass breakdown for this mission design. CBE refers to the current best estimate of the dry mass. The contingency masses are derived from [27, 28, 36]. Propellant mass is calculated as the mass necessary to perform all maneuvers for the CBE + contingency mass of each component. All propellant calculations use an  $I_{sp} = 235$  seconds.

Impactor	CBE	402 kg
	Contingency	40 kg (10%)
	Propellant	925 kg
	Prop. Contingency	93 kg (10%)
	Total	1460 kg
Observer	CBE	316 kg
	Contingency	104 kg (33%)
	Propellant	523 kg
	Prop. Contingency	52 kg (10%)
Total	995 kg	
<b>Total</b>		<b>2455 kg</b>
<b>Falcon 9 Launch</b>		<b>2655 kg</b>
<b>Mass Margin</b>		<b>200 kg</b>

Impact occurs to better estimate  $\beta$  before impact. This data not only helps to complete the mission goals, but also has significant scientific value, as studying the interiors of solid bodies is among the recent planetary science decadal's priority science questions [37]. Studying the interior of the secondary is particularly important to this mission, as the relevant interior forces of asteroids include non-negligible cohesion along with the gravity resulting from the distinct boulders and rubble that make them up [38, 39]. While the inclusion of cohesive forces may not greatly alter the effects of an impact, studying them has scientific importance and can be used to better model the history of the secondary [40]. In addition to radio wave mapping, the observer will thermally image the surface of the secondary with a 20 meter spatial resolution and  $\lambda/\Delta\lambda = 200$  spectral resolution [34]. Although the strength of the contact binary interface won't be directly measured, the thermal imaging will provide insight to the processes that the impact created and determine how the surface and subsurface were altered [41, 42].

The gravity field created by the binary system can be determined in multiple ways. In one method, we track where ejecta disperses around the binary system, specifically measuring where particles travel and deriving the gravity field from their trajectories. This method has been used before to great effect on the OSIRIS-REx mission when the asteroid Bennu was ejecting particles from its surface [43, 44]. Though this method can certainly be used after impact, it is unlikely to be of use for predicting density before impact. Another method is based on measuring the trajectories of the observer spacecraft and lander in the system and using their perturbed motion to determine the gravity field. That is, the spacecraft will be controlled precisely and will experience perturbations. Comparing these perturbations with the designed trajectory of the spacecraft, given enough measurements, allows us to determine the masses and bulk densities of the primary and secondary.

Determining  $\beta$  after the impact will require understanding the masses of the two bodies and will be helped by mapping the ejecta plume created by the impact. Thus, understanding the

gravity field is only the first step towards understanding the processes that we are causing. Perhaps most important to measuring  $\beta$  is determining what the secondary's path is after impact. As shown in Figure 6, the trajectory of the secondary after impact is highly dependent on  $\beta$ . Certainly, with knowledge of the interior of the secondary provided by the observer spacecraft, an expected  $\beta$  should be estimated before impact. This mission provides an opportunity to test our best estimates of  $\beta$ , including significant known information about the system, against a readily measurable impact.

### 3. Mechanics of Kinetic Impact

#### 3.1. 2002 AW Density and Mass

There is little available information on the mass of the two asteroids and, in available data sets, the densities are only assumed [29]. Knowledge of the mass is critical, as it is linearly related to the asteroid's momentum change provided by the impacting spacecraft. We determine the density of 2002 AW using Equation 1 and the masses then are easily determined. For the target asteroid 2002 AW, we derive the masses of the primary and secondary asteroid to be  $1.006\text{E}+10$  kg and  $1.034\text{E}+8$  kg, respectively. We determine  $\mu$  to be  $0.6783$  m<sup>3</sup>/s<sup>2</sup> and the density of each body to be  $1579.1$  kg/m<sup>3</sup>. Based on lightcurve data, it is known that 2002 AW is a B-class asteroid [31]. B-class asteroids have a reported average density of  $2190 \pm 1000$  kg/m<sup>3</sup> which our derived density also agrees with [45]. Though these derived quantities are used throughout this paper and are current best estimates, they are not measured and therefore may not accurately represent the actual binary system. To conclusively derive these values with precision, a detailed shape model and more data on the secondary's orbit are necessary. We note that even with the DART mission to Didymos and Dimorphos, the densities of the two objects are still uncertain [21]. Conversely, the observer spacecraft in this mission will help to determine the densities of the two asteroids before impact, as this is a capability that the DART mission did not have.

#### 3.2. Investigation of Impact

The full momentum transfer of the spacecraft impacting the secondary asteroid is represented as

$$m_s \mathbf{V}_i + m_{sc} \mathbf{V}_{sc} = (m_s + m_{sc} - m_{ejecta}) \mathbf{V}_f + m_{ejecta} \mathbf{V}_{ejecta} \quad (9)$$

where  $m_s$  is the mass of the secondary,  $\mathbf{V}_i$  is the initial velocity vector of the secondary with respect to the primary,  $m_{sc}$  is the spacecraft mass,  $\mathbf{V}_{sc}$  is the spacecraft's impacting velocity with respect to the primary,  $m_{ejecta}$  is the sum of the ejected mass,  $\mathbf{V}_f$  is the final velocity of the secondary after impact with respect to the primary, and  $\mathbf{V}_{ejecta}$  is the ejecta's average velocity vector. However,  $m_{ejecta}$  and  $\mathbf{V}_{ejecta}$  are completely unknown in the system. Instead of solving for both of these quantities and drastically increasing the error in our calculations, we introduce the multiplicative momentum factor  $\beta$ , as introduced in Section 1.2, and defined as

$$\beta = \frac{m_{ejecta} (\mathbf{V}_{ejecta} - \mathbf{V}_f)}{m_{sc} \mathbf{V}_{sc}} + 1 \quad (10)$$

such that  $\beta = 1$  is a perfectly inelastic collision. The  $\beta$  factor for this collision has not been analytically approximated, as this calculation would require significantly more knowledge of 2002 AW than is currently available. Instead, we will present a range of  $\beta$  factors and impact angles for which our previously specified spacecraft and trajectory will result in a collision. The final velocity vector  $\mathbf{V}_f$  of the secondary asteroid is given by

$$\mathbf{V}_f = \frac{m_s \mathbf{V}_i + \beta m_{sc} \mathbf{V}_{sc}}{m_s + m_{sc}} \quad (11)$$

which is a rearrangement of Equation 9 while accounting for  $\beta$ .

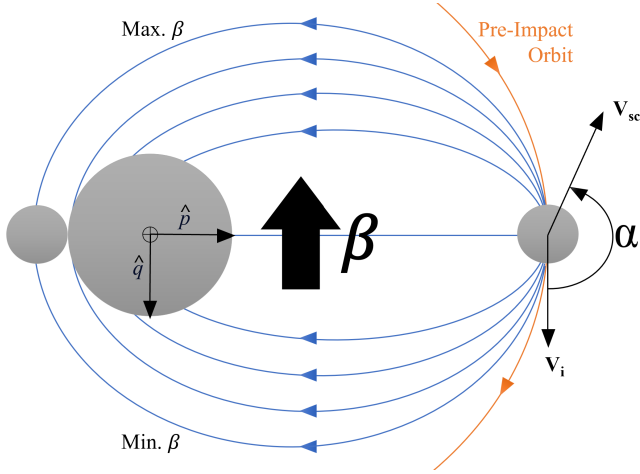


Figure 6: The secondary asteroid's orbit before the impact (orange) and after the impact (blue) depending on the  $\beta$  factor. The maximum and minimum cases will both have the same impact point which is represented by the asteroid on the left of the figure. As  $\beta$  increases, the final orbit will look more like the orbits on the top of the figure. Bounds for the maximum  $\beta$  and minimum  $\beta$  are provided in Figure 7, as they are dependent on  $\alpha$ . The impact angle  $\alpha$  is measured between the asteroid's pre-impact velocity vector  $\mathbf{V}_i$  and the spacecraft's impact velocity vector  $\mathbf{V}_{sc}$  and is defined in Equation 14.

We define the inertial perifocal frame such that the three vector components are: the unit vector from the primary asteroid to the secondary at impact  $\hat{p}$ , the velocity unit vector of the secondary at impact  $\hat{q}$ , and the angular momentum unit vector of the secondary about the primary  $\hat{w}$ . The state of the asteroid in this frame during impact is

$$\mathbf{r}_s = a_i \hat{p} \quad (12)$$

$$\mathbf{V}_i = \sqrt{\frac{\mu}{a_i}} \hat{q} \quad (13)$$

where  $a_i$  is the pre-impact semi-major axis. We define  $\alpha$  as

$$\alpha = \begin{cases} \arccos\left(\frac{\mathbf{V}_i \cdot \mathbf{V}_{sc}}{\|\mathbf{V}_i\| \|\mathbf{V}_{sc}\|}\right) & \text{if } \mathbf{V}_{sc} \cdot \hat{q} > 0 \\ -\arccos\left(\frac{\mathbf{V}_i \cdot \mathbf{V}_{sc}}{\|\mathbf{V}_i\| \|\mathbf{V}_{sc}\|}\right) & \text{if } \mathbf{V}_{sc} \cdot \hat{q} < 0 \end{cases} \quad (14)$$

so that the velocity of the spacecraft at the point of impact is

$$\mathbf{V}_{sc} = \begin{bmatrix} V_\infty \sin(\alpha) \\ V_\infty \cos(\alpha) \\ 0 \end{bmatrix} \quad (15)$$

where the magnitude of  $\mathbf{V}_{sc}$  is  $V_\infty$  in this form. As discussed in Section 2.1, the gravitational energy of the binary system

is negligible with respect to the impactor's kinetic energy and so we assume that  $\|\mathbf{V}_{sc}\| = V_\infty$ . As such, the final velocity vector of the secondary with respect to the primary,  $\mathbf{V}_f$ , can be represented as

$$\mathbf{V}_f = \frac{m_s}{m_s + m_{sc}} \begin{bmatrix} 0 \\ \sqrt{\frac{\mu}{a_i}} \\ 0 \end{bmatrix} + \beta \frac{m_{sc}}{m_s + m_{sc}} \begin{bmatrix} V_\infty \sin(\alpha) \\ V_\infty \cos(\alpha) \\ 0 \end{bmatrix} \quad (16)$$

in the perifocal frame. Because the position and velocity vectors are known for the moment of impact, we can now compute the semi-major axis  $a_f$ , the eccentricity vector  $\mathbf{e}$ , and the radius of periapsis  $r_p$

$$a_f = \frac{\mu \|\mathbf{r}_s\|}{2\mu - \|\mathbf{V}_f\|^2 \|\mathbf{r}_s\|} \quad (17)$$

$$\mathbf{e} = \frac{\mathbf{V}_f \times (\mathbf{r}_s \times \mathbf{V}_f)}{\mu} - \frac{\mathbf{r}_s}{\|\mathbf{r}_s\|} \quad (18)$$

$$r_p = a_f(1 - \|\mathbf{e}\|) \quad (19)$$

for the secondary after impact. To obtain a range of  $\beta$  and  $\alpha$  for which the secondary and primary asteroids collide, the radius of periapsis must be less than the radius of the primary and secondary asteroids (i.e.  $r_p < r_{imp}$ ).

The radius of periapsis for all combinations of  $1 \leq \beta \leq 6$  and  $90^\circ \leq \alpha \leq 270^\circ$  are displayed on Figure 7. The radius of impact is shown as the black contour lines on the plot. This impact radius is a conservative estimate, as the asteroids will not be perfect spheres and the 140 meters is a sum of the radii of the asteroids (25 meters for the secondary and 115 meters for the primary). Based on this model, the bounds for  $\beta$  for which the primary will impact the secondary are  $1.13 \leq \beta \leq 5.34$  at  $\alpha = 180^\circ$ . We do emphasize that these bounds can be drastically increased with a different target, as was discussed in Section 2.1. In Figure 7, the entire area encapsulated by the two black bands represents a high confidence collision result for the two asteroids after impact. The lower band denotes the case where the spacecraft impact delivers barely enough momentum to the secondary that they contact. The upper band denotes the case where the spacecraft impact delivers the maximum momentum to the secondary.

We then determine the contact speed of the secondary into the primary analytically using

$$V_{imp} = \sqrt{\frac{2\mu}{r_{imp}} - \frac{\mu}{a_f}} \quad (20)$$

which can be determined for the entire parameter space. We represent the case where  $\alpha = 180^\circ$  (perfectly tangential impact) in Figure 8, as this is what we focus on in this case study. The impact speed is less than escape speed, as is required for a body in an elliptical orbit, and so this impact should create a contact binary.

## 4. Discussion

### 4.1. The Catastrophic Disruption Limit

A kinetic impactor is capable of catastrophically disrupting a small body (causing it to lose 50% of its mass) if it hits with

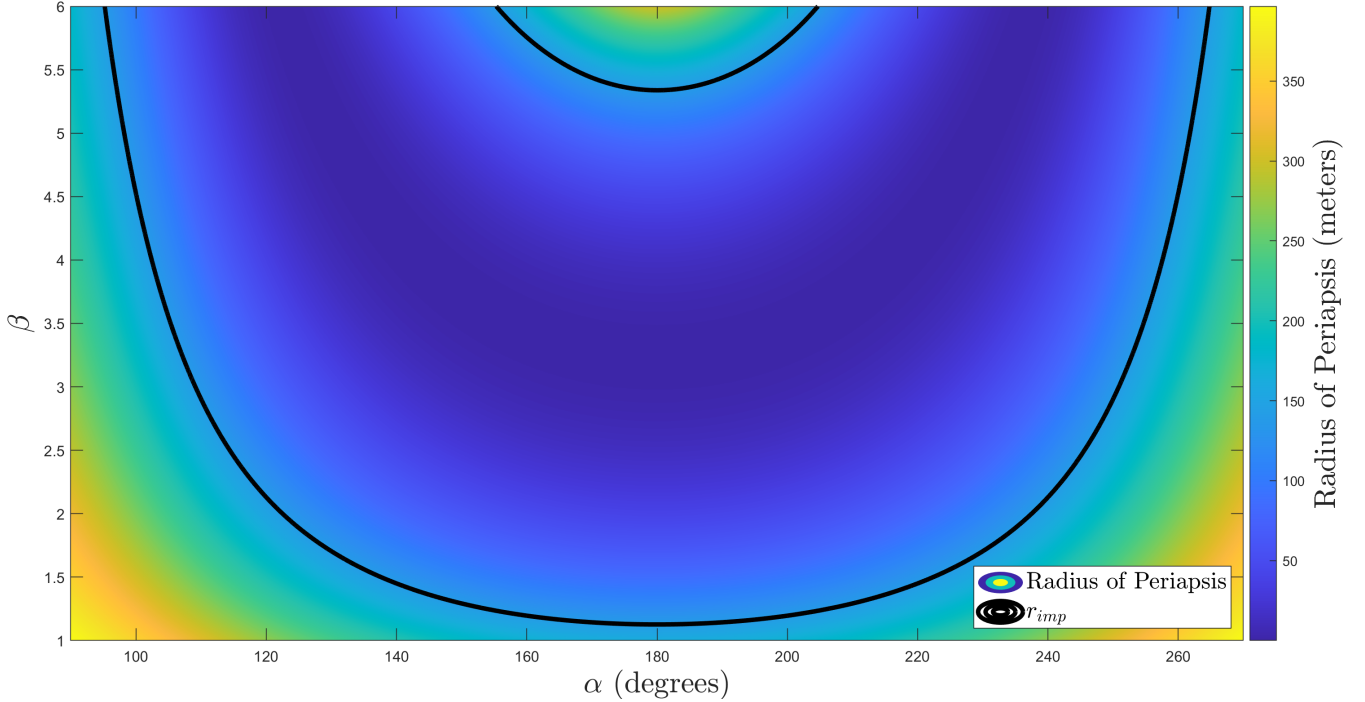


Figure 7: The contour measures the radius of periapsis of the secondary after the spacecraft impact in meters. The  $\beta$  value is measured on the y axis and the impact angle  $\alpha$  between the asteroid's velocity vector  $\mathbf{V}_i$  and the spacecraft's velocity vector  $\mathbf{V}_{sc}$  are on the x axis. The black contour lines on this graph represent the impact radius which is the sum of the primary and secondary asteroid's radii ( $r_{imp}$ ). The actual impact radius is expected to be larger, as the asteroids should be irregularly shaped and so these bounds have an inherent safety factor added to them. This graph was created assuming an impacting spacecraft mass of 483 kg and  $\mathbf{V}_{\infty} = 2.391$  km/s.

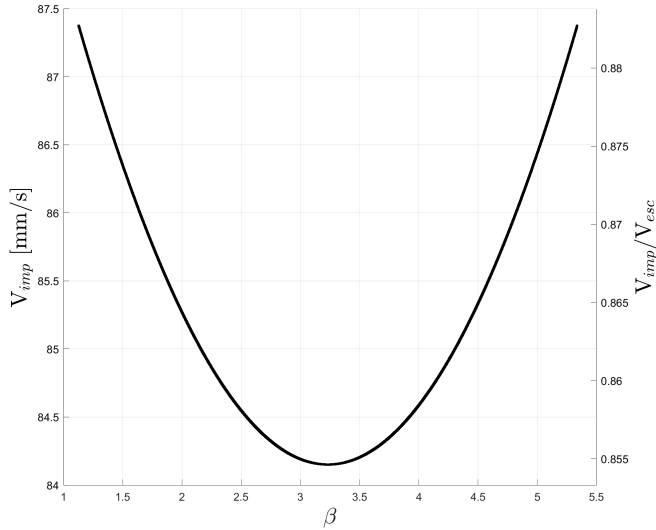


Figure 8: The impact speed of the secondary into the primary. The right y-axis gives the impact speed as a value normalized by the escape velocity. For  $\beta$  outside of the represented values, the contact binary will not form and therefore the impact speed is not applicable.

sufficient energy. For our chosen small body with a 25 meter radius, a conservative estimate of the catastrophic disruption limit is  $Q^* = 90$  J/kg where  $Q^*$  is the critical kinetic energy of the impactor divided by the mass of the target for which more than 50% of the target's mass will be lost [46]. With our impactor of 483 kg traveling at a relative impact speed of 2.391 km/s and our derived secondary mass of  $1.034E+8$  kg, we find that our impact will deliver 13.35 J/kg to the target, or approximately 14.8% of the catastrophic disruption limit. Though we expect that the asteroid should not catastrophically

disrupt, a significant percentage of the secondary's mass will be ejected. In the DART mission, the impactor delivered 2.54 J/kg to the target, approximately 2.8% of the catastrophic disruption limit, and caused 0.3%-0.5% of Dimorphos' mass to be ejected [32, 23].

#### 4.2. Mission Assurance

The greatest uncertainty in this mission is the  $\beta$  factor. We use Figure 7 as a design tool to optimize  $\beta$  bounds and compare these bounds to other studies to provide mission assurance. The bounds for  $\beta$  to cause the secondary to impact the primary,  $1.13 \leq \beta \leq 5.34$ , cover a wide range of asteroid properties. The prediction for  $\beta$  before the DART mission's impact was between 1 and 5 and predictions for  $\beta$  only exceeded 5 in edge cases with an extremely low coefficient of friction and material strength/cohesion [47]. After the impact, the DART team reported bounds  $2.2 \leq \beta \leq 4.9$  when accounting for uncertainty in the density of Dimorphos which validated the predictions [21]. Assuming an equal density for Didymos and Dimorphos,  $\beta = 3.61^{+0.19}_{-0.25}$  with  $1\sigma$  bounds which was a common result for cases where the cohesion was less than 10 MPa in the prediction tests [47]. The effect of cohesion on  $\beta$  is significant and increasing cohesion will decrease  $\beta$ . We take values from Bennu into consideration because it is expected that our target asteroid is a B-type and a rubble pile, as is the asteroid Bennu. Bennu has a cohesion of less than 1 Pa and material strengths of 0.1-0.8 MPa [48, 49]. Despite these values being very small, we do not expect that they will result in  $\beta$  being greater than 5 because impact velocity also has a significant effect on  $\beta$ ; decreasing impact velocity will decrease the  $\beta$  factor [18]. In mod-

els of impacts to Bennu, it was estimated that impact velocities less than 25 km/s (i.e. up to an order of magnitude greater than our impact velocity) would cause the  $\beta$  values to be less than 5 [50]. For cohesion of 1 kPa and material strengths between 1 kPa and 100 MPa, an impact at our impactor speed should not yield a  $\beta$  value greater than 3.5. For a porosity of 40% and an impact speed of 10 km/s, any cohesion in the range of 1 kPa to 100 MPa did not yield a  $\beta$  value greater than 3.5. When accounting for all of these previous simulations, we argue that the  $\beta$  value that our kinetic impactor will produce should fall into the bounds  $1.13 \leq \beta \leq 5.34$ . That is, we expect to create a contact binary. Part of our future work will be further validating this expectation through simulations for our specific target using the little known data about it.

#### 4.3. The Ideal Target

Of the list of systems we considered, 2002 AW was the best target for this mission. However, it should not be viewed as the ideal target for this mission. A truly ideal target would be different from 2002 AW in that it would: have a smaller system semi-major axis relative to primary and secondary size so that the range of  $\beta$  values that would result in collision increases (i.e. 2018 TF3), have a moderate to high albedo so that it is easier to observe for the fast-approaching impactor (i.e. Didymos), and have multiple chances for radiometric observations before the mission to determine a shape model for at least the primary asteroid (i.e. Moshup). Though 2002 AW fails on these attributes, it does have other aspects that make it an attractive target such as: a 50 meter diameter secondary which is the minimum size for which a kinetic impactor would be practically used, a minimal rendezvous  $\Delta V$  from LEO, and an easily attainable  $V_\infty$  value necessary for contact binary creation. The likelihood that an NEO fulfills all of these criteria is very small but it is possible. Because the ideal asteroid for this mission is likely very small (primary diameter  $< 250$  m), it is possible that an asteroid is known but its secondary has not yet been discovered. We reason that this is possible because 2002 AW's secondary was first discovered only recently in March 2022, 20 years after the primary was discovered, and it ended up as the target for this mission design.

## 5. Conclusion

This mission would provide the ability to closely observe a contact binary formation and would characterize a contact binary at all stages in its formation process. A binary system provides the perfect natural laboratory to carry out this mission, as was true of the DART mission. Not only does the analysis suggest this mission is achievable, but its technology risk is low, as are its launch and spacecraft-development costs. It leverages existing technology in both the impactor and observer spacecraft of the mission and requires only a single Falcon 9 launch.

This mission serves both the planetary defense community and planetary science community. The secondary of 2002 AW has the minimum diameter for which a kinetic impactor would be used for planetary defense (50 meters) and so this mission

provides a test of the ability to deflect small objects without causing catastrophic disruption. This mission would rapidly determine the  $\beta$  factor after impact by using data from the observer spacecraft and add to the still-uncertain understanding of expected  $\beta$  factors for impacts to arbitrary objects. Understanding the strength of contact binaries, specifically near their contact interface, is both scientifically valuable and highly applicable knowledge when deflecting hazardous contact binaries or binary systems.

## 6. Acknowledgements

The authors thank Brent W. Barbee, Justin Atchison, Megan Bruck Syal, and Pruthvi Banginwar for their guidance and recommendations. The authors also thank Dawn Grainger, Nancy Chabot, Andy Cheng, and Ron Ballouz for their helpful comments.

## References

- [1] J. L. Margot, M. C. Nolan, L. A. M. Benner, S. J. Ostro, R. F. Jurgens, J. D. Giorgini, M. A. Slade, D. B. Campbell, Binary asteroids in the near-earth object population, *Science* 296 (5572) (2002) 1445–1448. doi: 10.1126/science.1072094.
- [2] A. Berdeu, M. Langlois, F. Vachier, First observation of a quadruple asteroid: Detection of a third moon around (130) elektra with sphere/ifs, *Astronomy & Astrophysics L4* (2022). doi:https://doi.org/10.1051/0004-6361/202142623.
- [3] M. Ćuk, Formation and destruction of small binary asteroids, *The Astrophysical Journal* 659 (1) (2007) L57. doi:10.1086/516572.
- [4] J. McMahon, D. Scheeres, Detailed prediction for the byorp effect on binary near-earth asteroid (66391) 1999 kw4 and implications for the binary population, *Icarus* 209 (2) (2010) 494–509. doi:https://doi.org/10.1016/j.icarus.2010.05.016.
- [5] W. B. McKinnon, D. C. Richardson, J. C. Marohnic, J. T. Keane, W. M. Grundy, D. P. Hamilton, D. Nesvorný, O. M. Umurhan, T. R. Lauer, K. N. Singer, S. A. Stern, H. A. Weaver, J. R. Spencer, M. W. Buie, J. M. Moore, J. J. Kavelaars, C. M. Lisse, X. Mao, A. H. Parker, S. B. Porter, M. R. Showalter, C. B. Olkin, D. P. Cruikshank, H. A. Elliott, G. R. Gladstone, J. W. Parker, A. J. Verbiscer, L. A. Young, The solar nebula origin of (486958) arrokoth, a primordial contact binary in the kuiper belt, *Science* 367 (6481) (2020). doi:10.1126/science.aay6620.
- [6] J. Marohnic, D. Richardson, W. McKinnon, H. Agrusa, J. DeMartini, A. Cheng, S. Stern, C. Olkin, H. Weaver, J. Spencer, Constraining the final merger of contact binary (486958) arrokoth with soft-sphere discrete element simulations, *Icarus* 356 (2021) 113824. doi:https://doi.org/10.1016/j.icarus.2020.113824.
- [7] H. Rickman, S. Marchi, M. F. A'Hearn, C. Barbieri, M. R. El-Maarry, C. Güttler, W.-H. Ip, H. U. Keller, P. Lamy, F. Marzari, M. Massironi, G. Naletto, M. Pajola, H. Sierks, D. Koschny, R. Rodrigo, M. A. Barucci, J.-L. Bertaux, I. Bertini, G. Cremonese, V. D. Deppo, S. Debei, M. D. Cecco, S. Fornasier, M. Fulle, O. Groussin, P. J. Gutiérrez, S. F. Hviid, L. Jorda, J. Knollenberg, J.-R. Kramm, E. Kürt, M. Küppers, L. M. Lara, M. Lazzarin, J. J. L. Moreno, H. Michalik, L. Sabau, N. Thomas, J.-B. Vincent, K.-P. Wenzel, Comet 67p/churyumov-gerasimenko: Constraints on its origin from osiris observations, *Astronomy & Astrophysics (A44)* (2015). doi:https://doi.org/10.1051/0004-6361/201526093.
- [8] M. Yoshikawa, A. Fujiwara, J. Kawaguchi, The nature of asteroid itokawa revealed by hayabusa, in: *Proceedings of the International Astronomical Union: Near Earth Objects, our Celestial Neighbors: Opportunity and Risk*, Vol. 2 of S236, Cambridge University Press, 2006, pp. 401–416. doi:https://doi.org/10.1017/S174392130700350X.
- [9] L. Benner, M. Nolan, S. Ostro, J. Giorgini, D. Pray, A. Harris, C. Magri, J. Margot, Near-earth asteroid 2005 cr37: Radar images and photometry of a candidate contact binary, *Icarus* 182 (2) (2006) 474–481. doi:10.1016/j.icarus.2006.01.016.

- [10] S. S. Sheppard, D. Jewitt, Extreme kuiper belt object 2001 qg298 and the fraction of contact binaries, *The Astronomical Journal* 127 (5) (2004) 3023–3033. doi:10.1086/383558.
- [11] R. K. Mann, D. Jewitt, P. Lacerda, Fraction of contact binary trojan asteroids, *The Astronomical Journal* 134 (3) (2007) 1133–1144. doi:10.1086/520328.
- [12] M. Čuk, D. Nesvorný, Orbital evolution of small binary asteroids, *Icarus* 207 (2) (2010) 732–743. doi:https://doi.org/10.1016/j.icarus.2009.12.005.
- [13] S. A. Jacobson, D. J. Scheeres, Dynamics of rotationally fissioned asteroids: Source of observed small asteroid systems, *Icarus* 214 (1) (2011) 161–178. doi:https://doi.org/10.1016/j.icarus.2011.04.009.
- [14] P. A. Taylor, J.-L. Margot, Tidal end states of binary asteroid systems with a nonspherical component, *Icarus* 229 (2014) 418–422. doi:https://doi.org/10.1016/j.icarus.2013.11.008.
- [15] M. Jutzi, E. Asphaug, The shape and structure of cometary nuclei as a result of low-velocity accretion, *Science* 348 (6241) (2015) 1355–1358. doi:10.1126/science.aaa4747.
- [16] E. Asphaug, C. B. Agnor, Q. Williams, Hit-and-run planetary collisions, *Nature* 439 (2006) 155–160. doi:https://doi.org/10.1038/nature04311.
- [17] A. Cheng, P. Michel, M. Jutzi, A. Rivkin, A. Stickle, O. Barnouin, C. Ernst, J. Atchison, P. Pravec, D. Richardson, Asteroid impact & deflection assessment mission: Kinetic impactor, *Planetary and Space Science* 121 (2016) 27–35. doi:https://doi.org/10.1016/j.pss.2015.12.004.
- [18] K. A. Holsapple, K. R. Housen, Momentum transfer in asteroid impacts. i. theory and scaling, *Icarus* 221 (2) (2012) 875–887. doi:https://doi.org/10.1016/j.icarus.2012.09.022.
- [19] S. Raducan, T. Davison, R. Luther, G. Collins, The role of asteroid strength, porosity and internal friction in impact momentum transfer, *Icarus* 329 (2019) 282–295. doi:https://doi.org/10.1016/j.icarus.2019.03.040.
- [20] M. Bruck Syal, J. Michael Owen, P. L. Miller, Deflection by kinetic impact: Sensitivity to asteroid properties, *Icarus* 269 (2016) 50–61. doi:https://doi.org/10.1016/j.icarus.2016.01.010.
- [21] A. F. Cheng, H. F. Agrusa, B. W. Barbee, A. J. Meyer, T. L. Farnham, S. D. Raducan, D. C. Richardson, E. Dotto, A. Zinzi, V. D. Corte, T. S. Statler, S. Chesley, S. P. Naidu, M. Hirabayashi, J.-Y. Li, S. Egl, O. S. Barnouin, N. L. Chabot, S. Chocron, G. S. Collins, R. T. Daly, T. M. Davison, M. E. DeCoster, C. M. Ernst, F. Ferrari, D. M. Graninger, S. A. Jacobson, M. Jutzi, K. M. Kumamoto, R. Luther, J. R. Lyzhof, P. Michel, N. Murdoch, R. Nakano, E. Palmer, A. S. Rivkin, D. J. Scheeres, A. M. Stickle, J. M. Sunshine, J. M. Trigo-Rodríguez, J.-B. Vincent, J. D. Walker, K. Wünnemann, Y. Zhang, M. Amoroso, I. Bertini, J. R. Brucato, A. Capannolo, G. Cremonese, M. Dall’Ora, P. J. D. Deshapriya, I. Gai, P. H. Hasselmann, S. Ieva, G. Impresario, S. L. Ivanovski, M. Lavagna, A. Lucchetti, E. M. Epifani, D. Modenini, M. Pajola, P. Palumbo, D. Perna, S. Pirrotta, G. Poggiali, A. Rossi, P. Tortora, M. Zannoni, G. Zanutti, Momentum transfer from the dart mission kinetic impact on asteroid dimorphos, *Nature* (2023). doi:https://doi.org/10.1038/s41586-023-05878-z.
- [22] J.-Y. Li, M. Hirabayashi, T. L. Farnham, J. M. Sunshine, M. M. Knight, G. Tancredi, F. Moreno, B. Murphy, C. Opitom, S. Chesley, D. J. Scheeres, C. A. Thomas, E. G. Fahnestock, A. F. Cheng, L. Dressel, C. M. Ernst, F. Ferrari, A. Fitzsimmons, S. Ieva, S. L. Ivanovski, T. Kareta, L. Kolokolova, T. Lister, S. D. Raducan, A. S. Rivkin, A. Rossi, S. Soldini, A. M. Stickle, A. Vick, J.-B. Vincent, H. A. Weaver, S. Bagnulo, M. T. Bannister, S. Cambioni, A. C. Bagatin, N. L. Chabot, G. Cremonese, R. T. Daly, E. Dotto, D. A. Glenar, M. Granvik, P. H. Hasselmann, I. Herreros, S. Jacobson, M. Jutzi, T. Kohout, F. L. Forgia, M. Lazzarin, Z.-Y. Lin, R. Lolachi, A. Lucchetti, R. Makadia, E. M. Epifani, P. Michel, A. Migliorini, N. A. Moskovitz, J. Ormö, M. Pajola, P. Sánchez, S. R. Schwartz, C. Snodgrass, J. Steckloff, T. J. Stubbs, J. M. Trigo-Rodríguez, Ejecta from the dart-produced active asteroid dimorphos, *Nature* (2023). doi:https://doi.org/10.1038/s41586-023-05811-4.
- [23] A. Graykowski, R. A. Lambert, F. Marchis, D. Cazeneuve, P. A. Dalba, T. M. Esposito, D. O. Peluso, L. A. Sgro, G. Blaclard, A. Borot, A. Malvache, L. Marfisi, T. M. Powell, P. Huet, M. Limagne, B. Payet, C. Clarke, S. Murabana, D. C. Owen, R. Wasilwa, K. Fukui, T. Goto, B. Guillet, P. Huth, S. Ishiyama, R. Kukita, M. Mitchell, M. Primm, J. Randolph, D. A. Rivett, M. Ryno, M. Shimizu, J.-P. Toullec, S. Will, W.-C. Yue, M. Camilleri, K. Graykowski, R. Janetzke, D. Janke, S. Kardel, M. Loose, J. W. Pickering, B. A. Smith, I. M. Transom, Light curves and colors of the ejecta from dimorphos after the dart impact, *Nature* (2023). doi:https://doi.org/10.1038/s41586-023-05852-9.
- [24] C. A. Thomas, S. P. Naidu, P. Scheirich, N. A. Moskovitz, P. Pravec, S. R. Chesley, A. S. Rivkin, D. J. Osip, T. A. Lister, L. A. M. Benner, M. Brozović, C. Contreras, N. Morrell, A. Rožek, P. Kušnirák, K. Hornoch, D. Mages, P. A. Taylor, A. D. Seymour, C. Snodgrass, U. G. Jørgensen, M. Dominik, B. Skiff, T. Polakis, M. M. Knight, T. L. Farnham, J. D. Giorgini, B. Rush, J. Bellerose, P. Salas, W. P. Armentrout, G. Watts, M. W. Busch, J. Chatelain, E. Gomez, S. Greenstreet, L. Phillips, M. Bonavita, M. J. Burgdorf, E. Khalouei, P. Longa-Peña, M. Rabus, S. Sajadian, N. L. Chabot, A. F. Cheng, W. H. Ryan, E. V. Ryan, C. E. Holt, H. F. Agrusa, Orbital period change of dimorphos due to the dart kinetic impact, *Nature* (2023). doi:https://doi.org/10.1038/s41586-023-05805-2.
- [25] S. Hernandez, B. W. Barbee, S. Bhaskaran, K. Getzandanner, Mission opportunities for the flight validation of the kinetic impactor concept for asteroid deflection, *Acta Astronautica* 103 (2014) 309–321. doi:https://doi.org/10.1016/j.actaastro.2014.04.013.
- [26] K. J. Walsh, Rubble pile asteroids, *Annual Review of Astronomy and Astrophysics* 56 (1) (2018) 593–624. doi:10.1146/annurev-astro-081817-052013.
- [27] European space agency: Aim spacecraft facts & figures (2022). URL [https://www.esa.int/Space\\_Safety/Hera/AIM\\_spacecraft\\_Facts\\_Figures](https://www.esa.int/Space_Safety/Hera/AIM_spacecraft_Facts_Figures)
- [28] B. Sarli, M. Ozimek, J. Atchison, J. Englander, B. Barbee, Nasa double asteroid redirection test (dart) trajectory validation and robustness, 2017.
- [29] W. R. Johnston, Asteroids with satellites, <https://www.johnstonsarchive.net/astro/asteroidmoons.html> (2022).
- [30] Small-body mission-design tool, <https://ssd.jpl.nasa.gov/tools/mdesign.html/interactive> (2023).
- [31] P. Pravec, P. Kusnirak, K. Hornoch, P. Fatka, H. Kucakova, J. Liandro, J. de Leon, M. Popescu, G. N. Simion, B. A. Dumitru, Central bureau of astronomical telegrams electronic telegram no. 5110: (350751) 2002 aw, <http://www.cbat.eps.harvard.edu/iau/cbet/005100/CBET005110.txt> (2022).
- [32] R. T. Daly, C. M. Ernst, O. S. Barnouin, N. L. Chabot, A. S. Rivkin, A. F. Cheng, E. Y. Adams, H. F. Agrusa, E. D. Abel, A. L. Alford, E. I. Asphaug, J. A. Atchison, A. R. Badger, P. Baki, R.-L. Ballouz, D. L. Bekker, J. Bellerose, S. Bhaskaran, B. J. Buratti, S. Cambioni, M. H. Chen, S. R. Chesley, G. Chiu, G. S. Collins, M. W. Cox, M. E. DeCoster, P. S. Ericksen, R. C. Espiritu, A. S. Faber, T. L. Farnham, F. Ferrari, Z. J. Fletcher, R. W. Gaskell, D. M. Graninger, M. A. Haque, P. A. Harrington-Duff, S. Hefter, I. Herreros, M. Hirabayashi, P. M. Huang, S.-Y. W. Hsieh, S. A. Jacobson, S. N. Jenkins, M. A. Jensenius, J. W. John, M. Jutzi, T. Kohout, T. O. Krueger, F. E. Laipert, N. R. Lopez, R. Luther, A. Lucchetti, D. M. Mages, S. Marchi, A. C. Martin, M. E. McQuaide, P. Michel, N. A. Moskovitz, I. W. Murphy, N. Murdoch, S. P. Naidu, H. Nair, M. C. Nolan, J. Ormö, M. Pajola, E. E. Palmer, J. M. Peachey, P. Pravec, S. D. Raducan, K. T. Ramesh, J. R. Ramirez, E. L. Reynolds, J. E. Richman, C. Q. Robin, L. M. Rodriguez, L. M. Rouffberg, B. P. Rush, C. A. Sawyer, D. J. Scheeres, P. Scheirich, S. R. Schwartz, M. P. Shannon, B. N. Shapiro, C. E. Shearer, E. J. Smith, R. J. Steele, J. K. Steckloff, A. M. Stickle, J. M. Sunshine, E. A. Superfin, Z. B. Tarzi, C. A. Thomas, J. R. Thomas, J. M. Trigo-Rodríguez, B. T. Trof, A. T. Vaughan, D. Velez, C. D. Walker, D. S. Wilson, K. A. Wortman, Y. Zhang, Successful kinetic impact into an asteroid for planetary defense, *Nature* (2023). doi:https://doi.org/10.1038/s41586-023-05810-5.
- [33] P. Michel, M. Küppers, A. C. Bagatin, B. Carry, S. Charnoz, J. de Leon, A. Fitzsimmons, P. Gordo, S. F. Green, A. Hérique, M. Juzi, Özgür Karatekin, T. Kohout, M. Lazzarin, N. Murdoch, T. Okada, E. Palomba, P. Pravec, C. Snodgrass, P. Tortora, K. Tsiganis, S. Ulamec, J.-B. Vincent, K. Wünnemann, Y. Zhang, S. D. Raducan, E. Dotto, N. Chabot, A. F. Cheng, A. Rivkin, O. Barnouin, C. Ernst, A. Stickle, D. C. Richardson, C. Thomas, M. Arakawa, H. Miyamoto, A. Nakamura, S. Sugita, M. Yoshikawa, P. Abell, E. Asphaug, R.-L. Ballouz, W. F. Bottke, D. S. Lauretta, K. J. Walsh, P. Martino, I. Carnelli, The esa hera mission: De-

- tailed characterization of the dart impact outcome and of the binary asteroid (65803) didymos, *The Planetary Science Journal* 3 (7) (2022) 160. doi:10.3847/PSJ/ac6f52.
- [34] P. Michel, A. Cheng, M. Küppers, P. Pravec, J. Blum, M. Delbo, S. Green, P. Rosenblatt, K. Tsiganis, J. Vincent, J. Biele, V. Ciarletti, A. Hérique, S. Ulamec, I. Carnelli, A. Galvez, L. Benner, S. Naidu, O. Barnouin, D. Richardson, A. Rivkin, P. Scheirich, N. Moskovitz, A. Thirouin, S. Schwartz, A. Campo Bagatin, Y. Yu, Science case for the asteroid impact mission (aim): A component of the asteroid impact & deflection assessment (aida) mission, *Advances in Space Research* 57 (12) (2016) 2529–2547. doi:https://doi.org/10.1016/j.asr.2016.03.031.
- [35] C. for Near Earth Object Studies, Accessible neas (2023). URL <https://cneos.jpl.nasa.gov/nhats/>
- [36] Gridded ion thrusters (next-c), <https://www1.grc.nasa.gov/space/sep/gridded-ion-thrusters-next-c/> (2023).
- [37] T. N. A. Press (Ed.), *Origins, Worlds, and Life: A Decadal Strategy for Planetary Science and Astrobiology 2023-2032*, 2022, Ch. 3 Priority Science Questions. doi:10.17226/26522.
- [38] D. Scheeres, C. Hartzell, P. Sánchez, M. Swift, Scaling forces to asteroid surfaces: The role of cohesion, *Icarus* 210 (2) (2010) 968–984. doi:https://doi.org/10.1016/j.icarus.2010.07.009.
- [39] C. Hartzell, X. Wang, D. Scheeres, M. Horányi, Experimental demonstration of the role of cohesion in electrostatic dust lofting, *Geophysical Research Letters* 40 (6) (2011) 1038–1042. doi:https://doi.org/10.1002/grl.50230.
- [40] Y. Zhang, P. Michel, O. S. Barnouin, J. H. Roberts, M. G. Daly, R.-L. Ballouz, K. J. Walsh, D. C. Richardson, C. M. Hartzell, D. S. Lauretta, Inferring interiors and structural history of top-shaped asteroids from external properties of asteroid (101955) bennu, *Nature Communications* 13 (2022) 4589. doi:https://doi.org/10.1038/s41467-022-32288-y.
- [41] Y. Shimaki, H. Senshu, N. Sakatani, T. Okada, T. Fukuhara, S. Tanaka, M. Taguchi, T. Arai, H. Demura, Y. Ogawa, K. Suko, T. Sekiguchi, T. Kouyama, S. Hasegawa, J. Takita, T. Matsunaga, T. Imamura, T. Wada, K. Kitazato, N. Hirata, N. Hirata, R. Noguchi, S. Sugita, S. Kikuchi, T. Yamaguchi, N. Ogawa, G. Ono, Y. Mimasu, K. Yoshikawa, T. Takahashi, Y. Takei, A. Fujii, H. Takeuchi, Y. Yamamoto, M. Yamada, K. Shirai, Y. Ichi Iijima, K. Ogawa, S. Nakazawa, F. Terui, T. Saiki, M. Yoshikawa, Y. Tsuda, S. ichiro Watanabe, Thermophysical properties of the surface of asteroid 162173 ryugu: Infrared observations and thermal inertia mapping, *Icarus* 348 (2020) 113835. doi:https://doi.org/10.1016/j.icarus.2020.113835.
- [42] T. Okada, T. Fukuhara, S. Tanaka, M. Taguchi, T. Arai, H. Senshu, N. Sakatani, Y. Shimaki, H. Demura, Y. Ogawa, K. Suko, T. Sekiguchi, T. Kouyama, J. Takita, T. Matsunaga, T. Imamura, T. Wada, S. Hasegawa, J. Helbert, T. G. Müller, A. Hagermann, J. Biele, M. Grott, M. Hamm, M. Delbo, N. Hirata, N. Hirata, Y. Yamamoto, S. Sugita, N. Namiki, K. Kitazato, M. Arakawa, S. Tachibana, H. Ikeda, M. Ishiguro, K. Wada, C. Honda, R. Honda, Y. Ishihara, K. Matsumoto, M. Matsuoka, T. Michikami, A. Miura, T. Morota, H. Noda, R. Noguchi, K. Ogawa, K. Shirai, E. Tatsumi, H. Yabuta, Y. Yokota, M. Yamada, M. Abe, M. Hayakawa, T. Iwata, M. Ozaki, H. Yano, S. Hosoda, O. Mori, H. Sawada, T. Shimada, H. Takeuchi, R. Tsukizaki, A. Fujii, C. Hirose, S. Kikuchi, Y. Mimasu, N. Ogawa, G. Ono, T. Takahashi, Y. Takei, T. Yamaguchi, K. Yoshikawa, F. Terui, T. Saiki, S. Nakazawa, M. Yoshikawa, S. Watanabe, Y. Tsuda, Highly porous nature of a primitive asteroid revealed by thermal imaging, *Nature* 579 (2020) 518–522. doi:https://doi.org/10.1038/s41586-020-2102-6.
- [43] D. S. Lauretta, C. W. Hergenrother, S. R. Chesley, J. M. Leonard, J. Y. Pelgrift, C. D. Adam, M. A. Asad, P. G. Antreasian, R.-L. Ballouz, K. J. Becker, C. A. Bennett, B. J. Bos, W. F. Bottke, M. Brozović, H. Campins, H. C. Connolly, M. G. Daly, A. B. Davis, J. de León, D. N. DellaGiustina, C. Y. D. d’Aubigny, J. P. Dworkin, J. P. Emery, D. Farnocchia, D. P. Glavin, D. R. Golish, C. M. Hartzell, R. A. Jacobson, E. R. Jawin, P. Jenniskens, J. N. Kidd, E. J. Lessac-Chenen, J.-Y. Li, G. Libourel, J. Licandro, A. J. Liounis, C. K. Maleszewski, C. Manzoni, B. May, L. K. McCarthy, J. W. McMahon, P. Michel, J. L. Molaro, M. C. Moreau, D. S. Nelson, W. M. Owen, B. Rizk, H. L. Roper, B. Rozitis, E. M. Sahr, D. J. Scheeres, J. A. Seabrook, S. H. Selznick, Y. Takahashi, F. Thuillet, P. Tricarico, D. Vokrouhlický, C. W. V. Wolner, Episodes of particle ejection from the surface of the active asteroid (101955) bennu, *Science* 366 (6470) (2019) eaay3544. doi:10.1126/science.aay3544.
- [44] J. W. McMahon, D. J. Scheeres, S. R. Chesley, A. French, D. Brack, D. Farnocchia, Y. Takahashi, B. Rozitis, P. Tricarico, E. Mazarico, B. Bierhaus, J. P. Emery, C. W. Hergenrother, D. S. Lauretta, Dynamical evolution of simulated particles ejected from asteroid bennu, *Journal of Geophysical Research: Planets* 125 (8) (2020) e2019JE006229. doi:https://doi.org/10.1029/2019JE006229.
- [45] B. Carry, Density of asteroids, *Planetary and Space Science* 73 (1) (2012) 98–118. doi:https://doi.org/10.1016/j.pss.2012.03.009.
- [46] K. Holsapple, K. Housen, The catastrophic disruptions of asteroids: History, features, new constraints and interpretations, *Planetary and Space Science* 179 (2019) 104724. doi:https://doi.org/10.1016/j.pss.2019.104724.
- [47] A. M. Stickle, M. E. DeCoster, C. Burger, W. K. Caldwell, D. Graninger, K. M. Kumamoto, R. Luther, J. Ormö, S. Raducan, E. Rainey, C. M. Schäfer, J. D. Walker, Y. Zhang, P. Michel, J. M. Owen, O. Barnouin, A. F. Cheng, S. Chocron, G. S. Collins, T. M. Davison, E. Dotto, F. Ferrari, M. I. Herreros, S. L. Ivanovski, M. Jutzi, A. Lucchetti, E. Martellato, M. Pajola, C. S. Plesko, M. B. Syal, S. R. Schwartz, J. M. Sunshine, K. Wünnemann, Effects of impact and target parameters on the results of a kinetic impactor: Predictions for the double asteroid redirection test (dart) mission, *The Planetary Science Journal* 3 (11) (2022) 248. doi:10.3847/PSJ/ac91cc.
- [48] K. J. Walsh, R.-L. Ballouz, E. R. Jawin, C. Avdellidou, O. S. Barnouin, C. A. Bennett, E. B. Bierhaus, B. J. Bos, S. Cambioni, H. C. Connolly, M. Delbo, D. N. DellaGiustina, J. DeMartini, J. P. Emery, D. R. Golish, P. C. Haas, C. W. Hergenrother, H. Ma, P. Michel, M. C. Nolan, R. Olds, B. Rozitis, D. C. Richardson, B. Rizk, A. J. Ryan, P. Sánchez, D. J. Scheeres, S. R. Schwartz, S. H. Selznick, Y. Zhang, D. S. Lauretta, Near-zero cohesion and loose packing of bennu’s near subsurface revealed by spacecraft contact, *Science Advances* 8 (27) (2022) eabm6229. doi:10.1126/sciadv.abm6229.
- [49] B. Rozitis, A. J. Ryan, J. P. Emery, P. R. Christensen, V. E. Hamilton, A. A. Simon, D. C. Reuter, M. A. Asad, R.-L. Ballouz, J. L. Bandfield, O. S. Barnouin, C. A. Bennett, M. Bernacki, K. N. Burke, S. Cambioni, B. E. Clark, M. G. Daly, M. Delbo, D. N. DellaGiustina, C. M. Elder, R. D. Hanna, C. W. Haberle, E. S. Howell, D. R. Golish, E. R. Jawin, H. H. Kaplan, L. F. Lim, J. L. Molaro, D. P. Munoz, M. C. Nolan, B. Rizk, M. A. Siegler, H. C. M. Susorney, K. J. Walsh, D. S. Lauretta, Asteroid (101955) bennu’s weak boulders and thermally anomalous equator, *Science Advances* 6 (41) (2020) eabc3699. doi:10.1126/sciadv.abc3699.
- [50] D. S. Dearborn, M. Bruck Syal, B. W. Barbee, G. Gisler, K. Greenough, K. M. Howley, R. Leung, J. Lyzhoft, P. L. Miller, J. A. Nuth, C. S. Plesko, B. D. Seery, J. V. Wasem, R. P. Weaver, M. Zebeny, Options and uncertainties in planetary defense: Impulse-dependent response and the physical properties of asteroids, *Acta Astronautica* 166 (2020) 290–305. doi:https://doi.org/10.1016/j.actaastro.2019.10.026.